Probing Magnetic order in EELS of Chromite Spinels using both Multiple Scattering (FEFF8.2) and DFT (WIEN2k)

D.A. Eustace[a,1], D.W. McComb[b], and A.J. Craven[a,*]

[a]Department of Physics and Astronomy, University of Glasgow, University Avenue, Glasgow, G12 8QQ, Scotland, United Kingdom

[b] Department of Materials and London Centre for Nanotechnology and, Imperial College London, London, SW7 2AZ, United Kingdom

[1]Renishaw Diagnostics Ltd, Glasgow G33 1AP, Scotland, United Kingdom

ABSTRACT

The electron energy loss near edge structure on the O K-edge from chromite spinels contains fine structure from the hybridisation of the O p-orbitals and the Cr d-orbitals. Unlike the aluminates, a non-spin polarised calculation of this fine structure differs significantly from experimental observations. This is due to the large magnetic moment on the Cr. Calculations using simplified collinear ordering of the spins and the local spin density approximation give much improved agreement. A real space multiple scattering formalism and a reciprocal space density functional formalism give results in substantial agreement. In general, the actual spin arrangement of these chromites is not known since they are typically frustrated magnetic systems with ordering temperatures in the 10 – 20K range. The calculations are based on the hypothesis that dynamic short range order persists to room temperature over the time scale of the interaction with the fast electron. However, it is possible that the observed effects are due to the strong paramagnetism present at room temperatures but which it is not possible to simulate accurately at present.

Keywords:

ELNES

Chromite spinels

Magnetic order,

Local spin density approximation

FEFF8.2

WIEN2k

1. Introduction

Electron energy loss spectroscopy (EELS) carried out in the transmission electron microscope (TEM) or scanning transmission electron microscope (STEM) is now firmly acknowledged as the only characterisation technique capable of providing information on chemical bonding and electronic structure on the nanometre and sub-nanometre length scales in the "bulk" of a sample (Egerton, 1996). Ionisation edges occur when the electron beam causes core electrons of the atoms in a sample to be excited into unoccupied energy levels. The energy loss region up to 40 eV above an ionisation edge onset is termed the energy loss near-edge structure (ELNES) and is closely related to the band structure or local density of states of the material. By recording absorption edges, we are effectively probing a partial density of states of a material, thereby gaining valuable insight into both the nature of bonding and the electronic properties of the material under investigation. In the case of the O K-edge considered here, the dipole selection rule means that it is essentially the p-DOS that is probed. With recent improvements to microscope technology such as lens aberration correctors and electron gun monochromators, EELS can be carried out at sub-nanometre spatial resolution and with an extremely high (~0.1-0.2 eV) energy resolution (Egerton, 2003). Use of ELNES as a technique for materials characterisation is growing in popularity, but the complex electron-specimen interactions involved in the process are still not fully understood. Supporting systematic experimental studies with theoretical simulations can give new insights into the mechanisms responsible for the characteristic ELNES of ionisation edges.

A systematic experimental investigation of a series of chromite spinels (ACr_2O_4 where A = Mg, Ni, Co, Zn) revealed that hybridisation between the chromium (Cr^{3+}) 3d-orbital states and oxygen 2p-orbital states generates complex fine structure in the oxygen K-edge ELNES

(Docherty, 2001). In contrast, varying the tetrahedral A-site cation type had only a minimal effect on spectral shape. Additional structure in the experimental oxygen K-edge ELNES, such as pre-peaks and shoulders on common peaks, was tentatively allocated to additional structural variations such as inversion and tetragonal distortions (Docherty et al., 2001).

Theoretical simulations of the oxygen K-edge ELNES of aluminate spinels, recorded in the same study, showed good agreement with experiment (Docherty et al., 2001). These calculations were performed using the real space multiple scattering code FEFF8.0. However, similar calculations of the oxygen K-edge in chromite spinels showed significant discrepancies from the experimental result, both in peak position and intensity. Calculations of the oxygen K-edge of magnesium chromite using a simple antiferromagnetic ordering arrangement of chromium cations resulted in a significant improvement in the level of agreement with experiment (McComb et al., 2003). These calculations, carried out using a non-commercial simulation program, made use of the local spin density approximation (LSDA) within density functional theory (DFT). The sensitivity of the ELNES to magnetic interactions is surprising since the Néel temperatures, T_N, of the chromite spinels studied are typically 10-15K. The experimental data used in this study was collected at room temperature. Neutron powder diffraction investigations have detected dynamic short range magnetic order (SRO) up to 10 x T_N in an analogous compound, zinc ferrite (Schiessl et al., 1996). A model in which dynamic SRO persists in chromite spinels to room temperature has been proposed (McComb et al., 2003). The short interaction time of the electron with the sample, relative to that of the comparatively slow neutron, may result in the dynamic SRO being detected to much higher temperatures in the TEM.

In this paper, the importance of including magnetic correlations in calculations of the oxygen K-edge ELNES from a series of spinels is investigated using two generally available simulation codes, FEFF8.2 (Ankudinov et al., 1998) and WIEN2k (Schwarz, 2003). Using two different codes allows any changes in calculated ELNES to be attributed to the input parameters rather than the calculation programs themselves, giving a true picture of the interactions responsible for the characteristic ELNES shapes observed. The relative merits of the two differing calculation schemes can also be investigated. Klie *et al* have used WIEN2k to identify changes in the oxygen K-edge ELNES of lanthanum cobaltate ($LaCoO_3$) with changing spin-state Klie et al. (2007) but, in general, the use of these codes to perform magnetic simulations has not been widely investigated. Here, it is shown that both codes can be used to model simple antiferromagnetic structures, which are approximations to the extremely complex magnetic structures present in the actual materials. The level of agreement with experimental data is seen to improve significantly when compared to non-magnetic simulations carried out with the same codes. We demonstrate the robustness of these codes by investigating a range of chromite spinels with different magnetic properties, compositions and crystallographic structures.

2. Experimental and simulation Methods

Details of the chromite spinels investigated and the EELS acquisition parameters have been published previously (Docherty et al., 2001). Briefly, spectra were collected on a VG microscopes HB5 cold field emission gun (FEG) scanning transmission electron microscope (STEM) operating at 100kV. A Gatan 666 parallel electron-loss spectrometer controlled by Gatan EL/P software was used with a collection half-angle of 12 mrad. The full width at half

maximum (FWHM) of the zero-loss peak was between 0.5 and 0.6 eV. All crystallographic parameters used in the following calculations were obtained by Rietveld refinement of neutron powder diffraction data from the samples investigated (Docherty, 2001). All spinels investigated in this study were found to be structurally fully normal, meaning all A-site cations reside on tetrahedral sites, and all Cr atoms reside on octahedral sites.

The starting point of all ELNES calculation methodologies is Fermi's golden rule which describes the probability of an electron being excited from a core state into a final unoccupied state by means of an expression for the cross-section for scattering from a point (**r**) (Eq. 1). The left hand quantity is the double differential cross-section for scattering in terms of the scattered intensity *I*, the scattering solid angle $d\Omega$, and the energy range of the incident electrons, *dE*.

$$\frac{d^2I}{d\Omega dE} = \frac{2\pi}{\hbar}\rho(E)\left(\frac{e^2}{\varepsilon_0}\right)^2\left|\frac{< f|\exp(i\mathbf{q}.\mathbf{r})|i >}{q^2}\right|^2 \qquad (1)$$

On the right hand side term, *i* and *f* are the initial and final state wavefunctions respectively, **q** is the momentum transfer from the scattering event and $\rho(E)$ is the density of states for final state electrons of energy *E*. $\hbar$ is defined as Planck's constant divided by 2π, *e* is the charge of an electron and ε_0 is the permittivity of free space. In real space multiple scattering theory, used in FEFF8.2, the above expression is re-expressed in terms of a one electron Green's function formalism which describes the propagation of a photoelectron wave from a point **r** to a point **r**′. By considering the surrounding coordination shells as an array of muffin-tin potentials, the interference effects on the scattered wave can be calculated. Extended fine structure well above the edge can be readily calculated from single scattering

events, whereas near edge structure must include multiple scattering effects from a much larger atomic cluster. Such multiple scattering calculations do not require a periodic array of atoms, and a series of calculations in which the number of coordination shells considered is systematically increased, can give an insight into important scattering events. Calculations were performed using cluster sizes of approximately 150 atoms, with potentials calculated self-consistently.

A second approach is to consider that ELNES can be directly related to the local density of states after extraction of the necessary transition matrix elements. The calculation of local density of states is well established through various methods which make use of the local density approximation (LDA) in DFT (Hohenberg and Kohn, 1964). WIEN2k uses the Full Potential Linearized Augmented Plane Wave method within DFT (Schwarz, 2003) to solve the Kohn-Sham equations (Kohn and Sham, 1965) for ground state electron density, total energy and energy bands of periodic solids in reciprocal space. The "TELNES" module included within the program package calculates the double differential scattering cross-section over a grid of energy loss values and scattering impulse vectors. This is then integrated to yield a single differential cross-section which may be differential with respect to either energy or impulse transfer. The angular dependence of scattering may be included in the simulation if so desired. In the cases presented here the experimental samples were polycrystalline, and no consideration is given to the orientation dependence of the ELNES.

The excitation of an electron from an atomic core leaves a "core hole" which can have a significant impact on the shape of the density of states and consequently may influence the shape of the ELNES spectrum (Keast et al., 2001). The influence of the core hole on unoccupied density of states is material dependent, and is related to the ability of core and

valence electrons to screen the increased effective nuclear charge from the higher energy unoccupied states. In FEFF8.2, the effect of including a core hole may be easily investigated without increasing calculation time. Calculations shown here using FEFF8.2 include a core hole but there is no significant difference if the core hole is not included, probably due to the screening of the core hole by the valence electron density from the transition metal *d*-DOS (Scott *et al,* 2001). Including a core hole using WIEN2k involves the formation of a supercell with lower symmetry and requires significant additional computing resources. Calculations shown here with WIEN2k do not include a core hole due to the particular constraints of producing a viable spinel supercell with appropriate symmetry – the size of the unit cell required to include the appropriate core hole to core hole distances becomes too computationally expensive for relevant results to be achieved. However, due to the lack of difference observed in the FEFF8.2 calculations between those including a core hole and those that did not, it is believed the comparison of the two techniques remains valid regardless of core hole use. The core hole FEFF8.2 calculations are included here to properly reflect the interactions in the experimental data.

All FEFF8.2 simulations shown here were calculated using an SCF cluster of ~150 atoms. For the WIEN2k simulations, calculations were performed using 1000 k-points and an Rkmax (kinetic energy cut-off) value of 6. The importance of these parameters are fully discussed in the paper by Eustace *et al* (2006), where the authors describe the relative lack of influence of these factors on calculated K-edge shape. The energy convergence tolerance for the SCF cycle was 0.01 eV, but changing this criterion was found to have a minimal effect on spectral shape. However, the use of a consistent convergence criterion is essential for an accurate determination of total energy. In this case a series of calculations in which the convergence criteria was decreased were used to ensure proper energy convergence had been

achieved. The final convergence criterion chosen gave a variance of less than 0.01eV per unit cell, i.e. decreasing the energy convergence value below 0.01 eV resulted in changes in total energy value of less than three significant figures..

Simulated data must be broadened to account for experimental conditions. There are three broadening mechanisms which must be considered: instrumental broadening, which arises from the limited spectrometer resolution and energy spread of the electron source, and broadening which arises from the finite lifetime of the initial and final electronic states, respectively (Müller and Wilkins, 1984; Muller et al., 1998). In both FEFF8.2 and WIEN2k, instrumental broadening is added after the completion of the calculation by convolving the calculated spectrum with a Lorentzian function.

The core hole generated by the electron excitation will decay by radiative or Auger electronic transitions from higher occupied energy levels. This process determines the initial state lifetime. The broadening of the experimental spectrum due to a core hole width, Γ_c, is uniform over all energies, and is given by Eq. 2 (Müller and Wilkins, 1984; Muller et al., 1998), where $\overline{F}(E)$ is the final broadened spectrum at energy E, and $F(E')$ is the initial unbroadened spectrum at energy E'.

$$\overline{F}(E) = \frac{\Gamma_c}{2\pi} \int_{-\infty}^{\infty} \frac{F(E')dE'}{(E-E')^2 + (1/4)\Gamma_c^2} \qquad (2)$$

This type of broadening is usually disregarded due to the larger effects of instrumental broadening and final state lifetime broadening (the contribution of core state broadening to final peak width is likely to be <0.1 eV). The excited electron in the final state loses energy by emitting plasmons or creating electron-hole pairs until it falls back to the Fermi level. This

process controls the final state lifetime, which adds an energy-dependent broadening to the final experimental spectrum. This means that the fine structure of the ELNES is dampened with increasing energy – fine structure tends to be lost at energies more than 10eV above the edge threshold. The final state lifetime broadening due to a final state width, $\Gamma_x(E)$, may be described by Eq. 3 (Muller et al., 1998), where $\overline{\overline{F}}(E)$ is the final broadened spectrum at energy E, and $\overline{F}(E')$ is the initial non-lifetime broadened spectrum at energy E'.

$$\overline{\overline{F}}(E) = \frac{1}{2\pi}\int_{-\infty}^{\infty} \frac{\Gamma_x(E')\overline{F}(E')dE'}{(E-E')^2 + \frac{1}{4}\Gamma_\chi(E')^2} \qquad (3)$$

FEFF8.2 automatically includes some measure of final state lifetime broadening within the calculation scheme, the approximate effect of which is to increase the amount of broadening applied to features as a function of the square of the energy above the edge onset, i.e. higher energy features are broadened more. No additional instrumental broadening has been included in the FEFF8.2 simulations shown here. The WIEN2k simulated spectra presented here have been broadened by 0.4eV to account for instrumental effects. Additionally, final state lifetime broadening has been applied using an external program, which estimates the final state width in Eq. 3 according to the random phase approximation (Pines and Nozieres, 1989), in which E_p is the plasmon energy, E_0 is the bottom of the valence band and E_F is the Fermi energy (Eq. 4).

$$\Gamma_\chi(E) = \frac{\pi^2\sqrt{3}}{128}E_p\left(\frac{E-E_F}{E_F-E_0}\right)^2 \qquad (4)$$

Fully normal spinels which have a unit cell of 14 atoms (i.e. two formula units) containing magnetic cations exclusively on the B-sites are magnetically frustrated systems (Greeden, 2001). Magnetic frustration arises when the geometry of a set of interacting spins forbids a full antiferromagnetic alignment in all directions. In a spinel, the B-sites are in tetrahedral arrangement to each other, and are therefore coordinated in a magnetically frustrated system. Spin interaction energy will be minimised when the four spins on each tetrahedron add to zero. This allows for many different variations of magnetic spin alignment, and hence the magnetic structure of an antiferromagnetic spinel can be extremely complicated and is not known in detail for most chromite spinels. Magnetic simulations must therefore include simplified magnetic correlations so that the calculation time remains computationally viable.

The simulations shown here do not include a calculation of absolute edge onset energy – the edge onsets have been manually shifted to coincide with the edge onset from the experimental data, which was accurately recorded (Docherty, 2001).

3. Simulation results

3.1 Magnesium chromite

Magnesium chromite is known to be antiferromagnetic (AFM) with $T_N \approx 16K$ (Shaked et al., 1970). The magnetic structure of magnesium chromite is complex and not yet fully understood. The magnetic transition observed at 16K is associated with a structural transition from a cubic phase (Fd***Error! Bookmark not defined.***$\bar{3}$m) to a distorted tetragonal structure ($I4_1/amd$) (Ehrenberg et al., 2002). Calculations have shown that the magnitude of the

structural change is too small (the *a* axis is extended by 0.343%) to significantly alter the oxygen K-edge ELNES shape (Eustace, 2006). As in all chromite spinels investigated here, the chromium ions on the octahedral sites of the spinel lattice have oxidation state +3, (electronic configuration [Ar] $3d^3$) meaning the three d-electrons singularly occupy the three t_{2g} orbitals with parallel spins. The vacant *d*-orbital states in the Cr t_{2g} level are available to hybridise with the oxygen 2p-orbitals. Any magnetic interactions between chromium atoms may therefore have a significant impact on oxygen K-edge ELNES.

For the calculations, the lattice and oxygen parameters used were 8.332 Å and 0.2612, respectively. AFM calculations using the programs FEFF8.2 and WIEN2k permit the use of only one set of parallel spins (i.e. direct antiparallel alignment in only one direction). Systems with canted spins or more than one magnetic propagation vector cannot be modelled. Therefore, in calculations of AFM magnesium chromite, a simple ordering system must be used. In the calculations shown in this section, magnetic ordering has been introduced to the calculation in such a way that each octant of B-sites (containing 4 chromium atoms at alternate corners of a cubic structural unit) has two spin-up chromium atoms and two spin-down chromium atoms (Fig. 1).

Figs. 2(a) and 2(b) compare non-spin polarised calculations of the oxygen K-edge ELNES of magnesium chromite performed using FEFF8.2 and WIEN2k respectively, with experimental data (Fig. 2(e)). The discrepancies between the experiment and theory are clear, and occur mostly in the energy region up to 10 eV beyond the edge onset. This region of the ELNES has been directly attributed to transitions to the states created by the mixing of the chromium 3d- and oxygen 2p-orbitals (Docherty et al., 2001), and is therefore most

susceptible to the changes in the chromium density of states which occur when magnetic ordering is considered.

In the AFM FEFF8.2 calculation (Fig. 2(c)), there is a significant improvement in agreement with experiment. Peaks A, B, C and D can all now be identified, although peaks B and C are more intense than in experiment. A similar improvement is observed in the WIEN2k calculation (Fig. 2(d)), but peak B now appears as a shoulder to peak A, and peak D is modelled less well. The additional peak immediately following peak D in the FEFF8.2 calculation is not seen in the WIEN2k calculation. Despite these discrepancies, the improvement in the fit to experiment when simple AFM order is included is clear. WIEN2k allows us to compare the total energies of the AFM and non-magnetic systems. In this case, the AFM ordered magnesium chromite structure was found to be 5.386 eV per unit cell (0.385 eV per atom in the unit cell) lower in energy than the non-magnetic case. As stated above, the magnetic structure used to simulate this structure has been chosen the basis of computational suitability and is a simple anti-parallel spin correlation. In reality, the spin system will consist of canted magnetic spins due to the magnetic frustration present in the lattice. These canted spins will self-arrange themselves as spin ‘spirals’ or ‘clusters’ and the true experimental system will correspondingly have a lower self-energy than that calculated here. This is likely to be true for all spinels investigated here. However, simulations of this ‘true’ magnetic structure requires advances in code and computing power for efficient calculation. In the meantime, the work shown here is a good approximation and can be considered as indicative of the trend from the generalized case of magnetic vs non-magnetic structures.

3.2 Zinc chromite

Zinc chromite is a fully normal cubic spinel, similar to magnesium chromite, and has lattice and oxygen parameters of 8.328 Å and 0.2616, respectively. The magnetic spin structure of zinc chromite is complicated and has been investigated by many groups as a classic example of a magnetically frustrated system (Lee et al., 2002; Martinho et al., 2001). In one such study, measurements of the magnetic form factor by inelastic neutron scattering were interpreted as revealing the formation of hexagonal 'spin clusters'. In this spin structure, groups of six spins self-organise into weakly interacting antiferromagnetic loops. The temperature at which these 'spin clusters' are seen to transform from short range interactions to long range 'AFM' order has been found to be 12K, and is associated with a slight tetragonal crystal distortion.

Fig. 3 shows a series of calculations of the oxygen K-edge ELNES of zinc chromite. Similar to the magnesium chromite case, both non-magnetic simulations (Figs. 3(a) and 3(b)) exhibit few features which correspond well to peaks in the experimental spectrum (Fig. 3(e)). The introduction of antiferromagnetic order in the same configuration as discussed for the magnesium chromite case again improves the fit to experiment. In the FEFF8.2 calculation (Fig. 3(c)), the result is very similar to the magnesium chromite case. Peaks A-E can be readily identified, although peaks B and C are again rather high in intensity when compared to experiment. In addition, the fine structure observed between peaks B and C in the experimental data is not observed.

Considering the WIEN2k simulation (Fig. 3(d)), peak B is again observed as a shoulder on the high energy side of peak A. Peak C can be identified, but is lower in energy than in

experiment, and an additional peak is observed between B and C. The shoulder on the low energy side of peak D is not easily seen, and an additional shoulder not seen in experiment is observed on the high energy side. The AFM ordered $ZnCr_2O_4$ is calculated as 4.755 eV per unit cell (0.340 eV per atom) lower in energy than the non-magnetic case.

3.3 Nickel chromite

Nickel chromite is a fully normal tetragonal spinel with lattice parameters a = 5.84398 Å, c = 8.41528 Å and oxygen parameters of 0.2645 and 0.4798. The tetragonal structure arises due to a Jahn-Teller effect on the nickel atoms on the tetrahedral A-site (Ueno et al., 1999; Ishibashi and Yasumi, 2007). This distortion removes the *d*-orbital degeneracy present in the system, moving the system to a lower energy structure. The nickel atoms on the A-sites have no unpaired electrons, and hence have no magnetic moment. Magnetic order only arises from the chromium atoms on the B-sites of the spinel lattice. Nickel chromite is known to be antiferromagnetic with $T_N \sim 74K$ (Tomiyasu and Kagomiya, 2004). An antiferromagnetic arrangement of chromium atoms has been introduced to the calculation in the same way as that described in the magnesium chromite case. The tetragonal distortion of the spinel lattice does not overly complicate the calculation due to the use of primitive unit cells in the magnetic calculations. In a tetragonal spinel, there are two crystallographically inequivalent oxygen sites. The oxygen K-edge ELNES is calculated separately for each site, and the two averaged to arrive at a final oxygen K-edge as presented in Fig. 3.

Again, the non-magnetic calculations (Figs. 4(a) and 4(b)) show large discrepancies with the experimental data (Fig. 4(e)). Considering the AFM FEFF8.2 simulation (Fig. 4(c)), all peaks can be readily identified, although peaks A-C have shifted to lower energies. Peak A

and B appear narrower than in experiment, but the additional structure of peak C may be observed. Peak D is reasonably well modelled, although it is narrower than in experiment. There is an additional peak on the high energy side of peak D which is not seen in experiment.

In the WIEN2k simulations (Fig. 4(d)), the width of peaks A and D are improved, although peaks B and C are still seen to shift to lower energies. The splitting of peak C is similar to that observed in the FEFF8.2 simulation. There is a shoulder on the high energy side of peak D not seen in experiment. The antiferromagnetic $NiCr_2O_4$ is found to be 4.925 eV per unit cell (0.352 eV per atom) lower in energy than in the non-magnetic case.

3.4 Cobalt chromite

Unlike the other spinels presented above, cobalt chromite is not a frustrated magnetic system since the cobalt atoms on the A-sites possess a magnetic moment. Cobalt chromite is therefore a ferrimagnetic normal cubic spinel. The lattice and oxygen parameters used were 8.332 Å and 0.2617, respectively. Simple ferrimagnets have antiparallel coordination of spins but with a majority of spins in one direction. However, the spin orientations in cobalt chromite are more complicated. The A and B-site spins are canted in such a way that a magnetic 'spiral' structure arises (Tomiyasu et al., 2004). Hence, the magnetic order can be separated into two components – a ferrimagnetic component and a spiral component.

The magnetic structure can be viewed as ferromagnetic below 97K. Lowering the temperature further, spiral ordering develops which causes the spin direction on each site to be tilted, lowering the overall magnetic moment, but not to zero as would be the case in an

antiferromagnetic alignment (Tomiyasu et al., 2004). The spiral component of the magnetisation results in an overall ferrimagnetic state, since the chromium and cobalt atoms have their spins canted in different directions, lowering the net magnetic moment. This cannot be modelled using FEFF8.2 and WIEN2k. A calculation performed using an antiparallel alignment of cobalt and chromium atoms (a conventional ferrimagnetic system) found this to be higher in energy than the ferromagnetic case. Therefore, cobalt chromite has been modelled as a simple ferromagnet, where the cobalt and chromium atoms have a parallel alignment of magnetic moments.

In both the FEFF8.2 and WIEN2k non-magnetic calculations (Figs. 5(a) and (b) respectively), there is no good agreement with the experimental spectrum (Fig. 5(e)). Peaks A and B cannot be readily identified, although peak C is modelled well in the WIEN2k case. The inclusion of ferromagnetic interactions in the simulation improves the fit to experiment in an analogous manner to the AFM cases presented above. The splitting of peak C, which is dependant upon A-cation type, is much more significant in the FEFF8.2 calculation (Fig. 5(c)). Peak C is more accurately modelled in the WIEN2k simulation (Fig. 5(d)). Peak D is featureless in both calculations, while in the experimental data there is a clear shoulder on the lower energy side. Both calculations show a pre-peak, "*", that is not present in the experimental spectrum. The ferromagnetic system was found to be 4.860 eV per unit cell (0.347 eV per atom) lower in energy than the non-magnetic case.

4. Discussion

Some general conclusions may be drawn from the series of simulations shown above. Structural and magnetic differences between spinel types did not alter the fit to experiment significantly with respect to peak intensity, shape and position. In the FEFF8.2 calculations, the fine structure allocated to states created by p-d bond hybridisation was generally found to be compressed into a smaller energy range than in experiment, and the peak width was consistently calculated narrower than observed in the experimental data. Further broadening would be required to obtain a better fit to experiment in terms of line width, but this would result in the loss of discrete peaks and shoulders which can be correlated to experimental data. In general, the results of the WIEN2k calculations showed a better fit to experiment than the results of the FEFF8.2 calculations. This is likely to be due to the improved calculation of the self consistent atomic potentials using the WIEN2k program. The magnetic correlation between potentials is perhaps better handled by the DFT calculation. WIEN2k calculations showed improved agreement with respect to line widths and peak energy separation in all cases. It is possible that the external broadening algorithms used on this data are also more effective than those built-in to the FEFF8.2 code.

The difference in calculation of self-consistent atomic potentials is also the likely explanation for the lack of agreement between the non-magnetic calculations from each of the codes. The effect of magnetic interaction is likely to be the dominant factor in determining the true oxygen K-edge shape (as observed by the fact that both codes yield similar AFM oxygen K-edges). But when this magnetic interaction is removed from the calculation, the differences in potential calculations are exposed as both programs calculate ‘wrong’ structures.

In the FEFF8.2 calculations of magnesium chromite and nickel chromite, additional peaks were observed on the high energy side of peak D, prior to peak E. These extra peaks are

common in FEFF8.2 calculations (Pailloux et al., 2005; van Aken et al., 2004), and have also been noted in WIEN2k calculations of the oxygen K-edge ELNES in some perovskites (Harkins, 2005). Their origin is unknown but, in this case, these peaks may arise from an artificial magnetic periodicity which results from the simplified magnetic structure. This periodicity may not be present in the experimental materials which have a complicated true magnetic structure. Extra peaks were also observed as shoulders in the WIEN2k calculations of nickel chromite and zinc chromite, although in these cases this may be due to an inaccurate treatment of lifetime broadening. WIEN2k final state lifetime broadening has been added by an external program using values which give the best fit to experiment in the region where p-d bond hybridisation effects are seen, i.e. the first 10eV above edge onset. The use of broadening in calculations of ELNES is not a well established technique. Greater understanding is required to ensure the correct parameters are used.

However, despite the discrepancies described above, the inclusion of magnetic order improved the fit to experiment in all cases, showing that magnetic correlations within these materials have a significant affect on the oxygen K-edge ELNES, confirming the previous conclusions from calculations of magnesium chromite using an LSDA calculation scheme within DFT (McComb et al., 2003). The origin of the magnetic interactions is not clear given the extremely low T_N of all spinels studied. Approximate calculations of the exchange energy between first nearest neighbour chromium cations using the Heisenberg model suggest that temperatures in excess of 800 K would be required to destroy all atomic length scale magnetic correlations.

There is an alternative origin of the magnetic correlations responsible for the characteristic oxygen K-edge ELNES shape that must be considered. The results of the non-magnetic

calculations shown here contain no treatment of magnetic moment, despite the fact that the chromium cations possess a strong magnetic moment at all temperatures due to the three unpaired electrons present. All chromite spinels described here display bulk paramagnetism at room temperature. Therefore, it is not known if the magnetic interactions discussed here must be included in calculations in the form of short range order or whether the presence of a random distribution of appropriate moments on each sub-lattice would give an accurate simulation of the experimental data.

Clearly, both an accurate simulation of the short range order magnetic structure described for zinc chromite and an accurate representation of paramagnetism would require consideration of a non-collinear spin system. However, almost all generally available simulation programs require a collinear spin arrangement. A version of the WIEN2k code capable of performing non-collinear spin polarised calculations has been released (Laskowski et al., 2004), but has only been used in the calculation of correlated spin systems such as spin spirals, and requires extensive computational resources. A true paramagnetic calculation would include no correlation between spins, significantly increasing the computational resources required.

5. Conclusions

In this paper we have demonstrated that the experimentally recorded oxygen K-edge ELNES from a series of chromite spinels may only be accurately simulated when appropriate magnetic interactions are included in the calculations. FEFF8.2 and WIEN2k, which are popular simulation codes commonly used for EELS simulations, can carry out such magnetic

calculations with a reasonable level of success. The results from the two codes show a high degree of consistency, despite the use of different calculation mechanisms.

The discrepancies that remain between the calculation results and the experimental data may be attributed to the limited knowledge of the appropriate type of magnetic interactions present in the materials at room temperature. Future work must involve investigations of short range ordered magnetic structures and bulk paramagnetism, but will require a non-collinear treatment of magnetic spin for an accurate reproduction of the true spin orientations present.

6. Acknowledgements

The authors wish to express their gratitude to Dr. F.T. Docherty for provision of the experimental data; Prof. A.T. Paxton of the Atomistic Simulation Centre, Queen's University, Belfast for provision of a lifetime broadening program; the Engineering and Physical Science Research Council (EPSRC) for a Doctoral Training Fund studentship (DAE).

References

Ankudinov, A.L., Ravel, B., Rehr, J.J., Conradson, S.D., 1998. Real Space Multiple Scattering Calculation of XANES. Physical Review B 58, 7565.

Docherty, F.T., 2001. ELNES Investigations of Spinels. PhD Thesis. University of Glasgow.

Docherty, F.T., Craven, A.J., McComb, D.W., Skakle, J, 2001. ELNES investigations of the oxygen K-edge in spinels. Ultramicroscopy 86, 273-288.

Egerton, R.F., 1996. Electron energy loss spectroscopy in the electron microscope. 2nd Edition ed., New York; London: Plenum Press

Egerton, R.F., 2003. New techniques in electron energy loss spectroscopy and energy-filtered imaging. Micron 34, 127-139.

Ehrenberg, H., Knapp, M., Baehtz, C., Klemme, S., 2002. Tetragonal low-temperature phase of $MgCr_2O_4$. Powder Diffraction 17, 230-233.

Eustace, D.A., Docherty, F.T., McComb, D.W., Craven, A.J., 2006. ELNES as a probe of magnetic order in mixed oxides. Journal of Physics: Conference Series 26, 165-168.

Eustace, D.A., 2006. Spin Polarisation Effects in Electron Energy Loss Spectroscopy. PhD Thesis University of Glasgow.

Greedan, J.E., 2001. Geometrically frustrated magnetic materials. Journal of Materials Chemistry 11, 37-53.

Harkins, P., 2005. EELS and ELNES Investigation of Titanate and Zirconate Perovskites. Thesis, University of Glasgow.

Hohenberg, P. and W. Kohn, 1964. Inhomogeneous Electron Gas. Physical Review 136, B864-B871.

Ishibashi, H. and T. Yasumi, 2007. Structural transition of spinel compound $NiCr_2O_4$ at ferrimagnetic transition temperature. Journal of Magnetism and Magnetic Materials 310, E610-E612.

Keast, V.J., Scott., A.J., Brydson, R., Williams, DB., Bruley, J., 2001. Electron energy loss near-edge structure - a tool for the investigation of electronic structure on the nanometre scale. Journal of Microscopy 203, 135-175.

Klie, R.F., Zheng, J.C., Zhu, Y., Varela, M., Wu, J., Leighton, C., 2007. Direct Measurement of the Low-Temperature Spin-State Transition in $LaCoO_3$. Physical Review Letters 99, 047203.

Kohn, W. and Sham, L.J., 1965. Self-Consistent Equations Including Exchange and Correlation Effects. Physical Review 140, A1133-A1138.

Laskowski, R., Madsen, G.K., Blaha, P., Schwarz, K-H., 2004. Magnetic structure and electric-field gradients of uranium dioxide: An ab initio study. Physical Review B 69, 140408.

Lee, S.H., Broholm, C., Ratcliff, W., Gasparovic, G., Huang, Q., Kim, T.H., Cheong, S.W., 2002. Emergent excitations in a geometrically frustrated magnet. Nature 418. 856-858.

Martinho, H., Moreno, N.O., Sanjurjo, J.A., Rettori, C., Garcia-Adeva, A.J., Huber, D.L., Oseroff, S.B., Ratcliff, W., Cheong, S.W., Pagliuso, P.G., Sarrao, J.L., Martins, G.B., 2001. Magnetic properties of the frustrated antiferromagnetic spinel $ZnCr_2O_4$ and the spin-glass $Zn_{1-x}Cd_xCr_2O_4$ (x=0.05,0.10). Physical Review B 64, 024408.

McComb, D.W., Craven, A.J., Chioncel, L, Lichtenstein, A.I., Docherty, F.T., 2003. Effect of short-range magnetic ordering on electron energy loss spectra in spinels. Physical Review B 68, 224420.

Muller, D.A., Singh, D.J., Silcox, J., 1998. Connections between the electron-energy loss spectra, the local electronic structure, and the physical properties of a material: A study of nickel aluminum alloys. Physical Review B 57, 8181-8202.

Müller, J.E. and Wilkins, J.W., 1984. Band-structure approach to the x-ray spectra of metals. Physical Review B 29, 4331-4348.

Pailloux, F., Jublot, M., Gaboriaud, R.J., Jaouen, M., Paumier, F., Imhoff, D., 2005. Interfacial phases in epitaxial growth of Y_2O_3 on MgO studied via combining electron energy loss spectroscopy and real-space self-consistent full multiple scattering calculations. Physical Review B 72, 125425.

Pines, D., Nozieres, P. 1989. The Theory of Quantum Liquids.Vol. 1. Addison-Wesley, New York.

Scott, A.J., Brydson, R., MacKenzie, M., Craven, A.J., 2001. Theoretical investigation of the ELNES of transition metal carbides for the extraction of structural and bonding information. Physical Review B 63, 245105.

Shaked, H., Hastings, J.M., Corliss, M., 1970. Magnetic Structure of Magnesium Chromite. Physical Review B 1, 3116-3124.

Schiessl, W., Potzel, W., Karzel, H., Steiner, M., Kalvius, G.M., 1996. Magnetic properties of the $ZnFe_2O_4$ spinel. Physical Review B 53, 9143-9152.

Schwarz, K., 2003. DFT calculations of solids with LAPW and WIEN2k. Journal of Solid State Chemistry 176, 319-328.

Tomiyasu, K. and Kagomiya, I., 2004. Magnetic structure of $NiCr_2O_4$ studied by neutron scattering and magnetization measurements. Journal of the Physical Society of Japan 73, 2539-2542.

Tomiyasu, K., Fukunaga, J., Suzuki, H., 2004. Magnetic short-range order and reentrant-spin-glass-like behavior in $CoCr_2O_4$ and $MnCr_2O_4$ by means of neutron scattering and magnetization measurements. Physical Review B 70, 214434.

Ueno, G., Sato, S., Kino, Y., 1999. The low-temperature tetragonal phase of $NiCr_2O_4$. Acta Crystallographica Section C-Crystal Structure Communications 55, 1963-1966.

van Aken, P.A., Hoche, T., Heyroth, F., Keding, R., Uecker, R., 2004. Insights into oxygen-cation bonding in fresnoite-type structures from OK- and Ti L-23-electron energy loss spectra and ab initio calculations of the electronic structure. Physics and Chemistry of Minerals 31, 543-552.

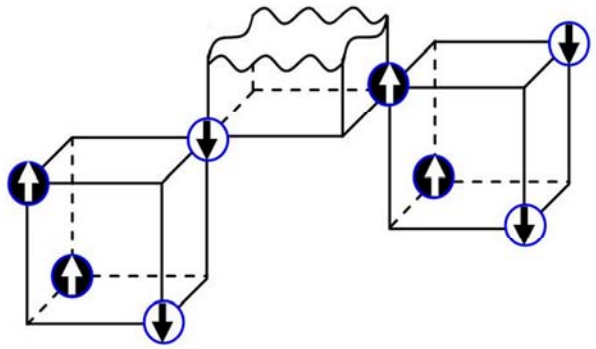

Fig. 1 Schematic of two octants in the spinel unit cell, showing the positions and spin orientations of the B-site cations in an antiferromagnetic alignment.

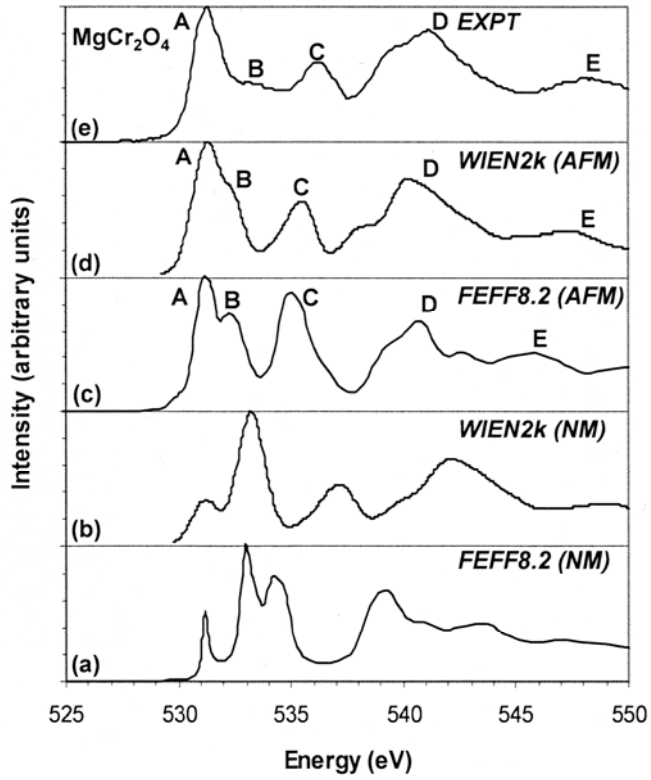

Fig. 2 The oxygen K-edge ELNES of $MgCr_2O_4$ calculated using non-magnetic (NM) (a, b) and antiferromagnetic (AFM) parameters (c, d) compared with experiment (e).

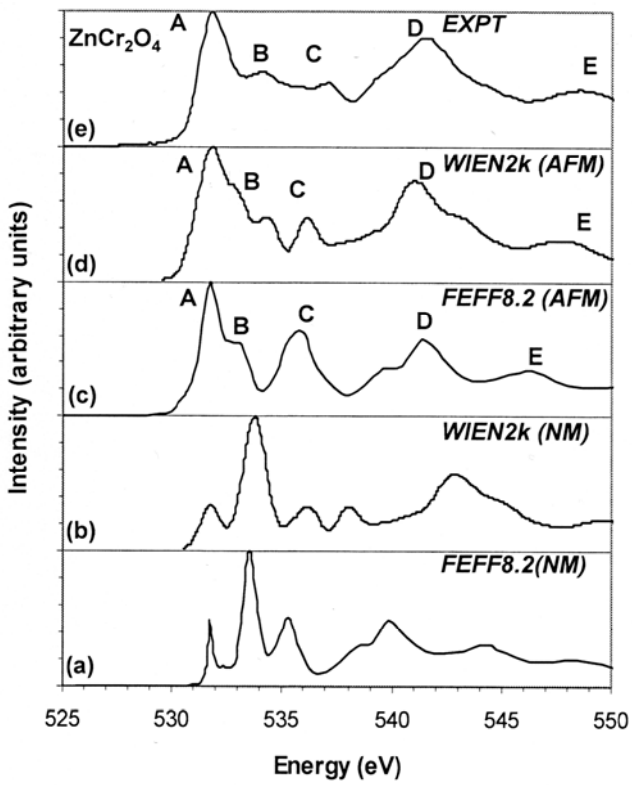

Fig. 3 The oxygen K-edge ELNES of $ZnCr_2O_4$ calculated using non-magnetic (NM) (a, b) and antiferromagnetic (AFM) parameters (c, d) compared with experiment (e).

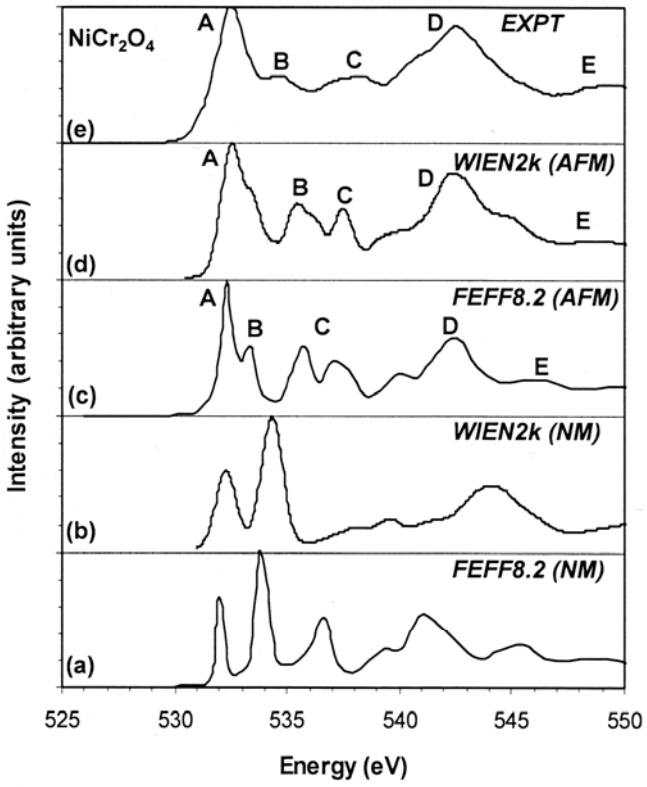

Fig. 4 The oxygen K-edge ELNES of tetragonal $NiCr_2O_4$ calculated using non-magnetic (NM) (a, b) and antiferromagnetic (AFM) parameters (c, d) compared with experiment (e).

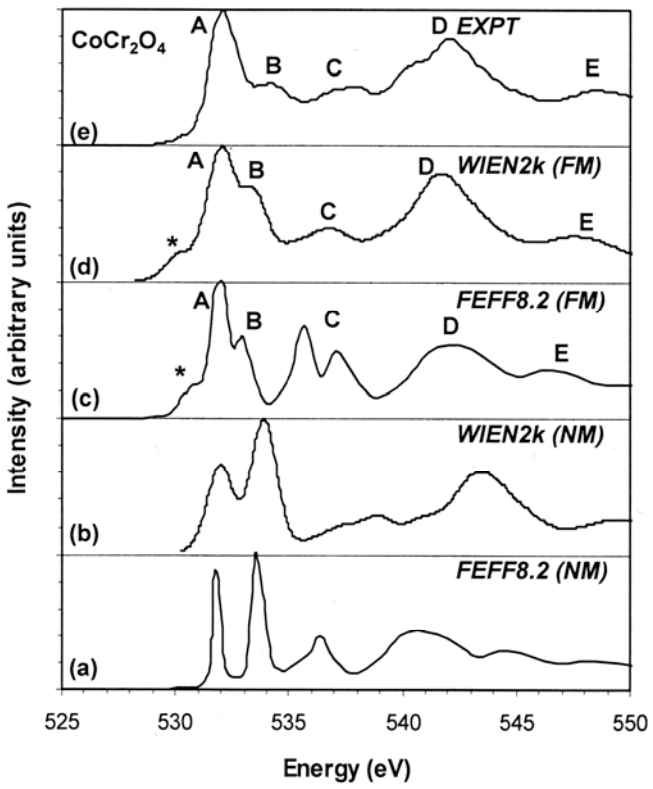

Fig. 5 The oxygen K-edge ELNES of $CoCr_2O_4$ calculated using non-magnetic (NM) (a, b) and ferromagnetic (FM) parameters (c, d) compared with experiment (e).